

Spatial patterns of phase in gamma EEGs from primary sensory cortices reveal the dynamics of mesoscopic wave packets**Walter J Freeman****To appear in: International Journal of Bifurcation and Chaos**

Department of Molecular & Cell Biology
University of California
Berkeley CA 94720-3200 USA
tel 510-642-4220 fax 510-643-6791
wfreeman@socrates.berkeley.edu

Submitted 10 December 2001 29 pages 17 Figures 3 Tables 10,383 words

Key words: EEG phase, gamma band, phase gradient, spatial pattern, state transition, theta band

Running title: Spatial phase cones in gamma EEGs

ABSTRACT

Domains of cooperative neural activity called 'wave packets' have been discovered in the visual, auditory, and somatomotor cortices of rabbits that were trained to discriminate conditioned stimuli in these modalities. Each domain forms by a first order state transition, which strongly resembles a phase transition from vapor to liquid. In this view, raw sense data injected into cortex by sensory axons drive cortical action potentials in swarms like water molecules in steam. The increased activity destabilizes the cortex. Within 3 to 7 milliseconds of transition onset, the activity binds together into a state resembling a scintillating rain drop, which lasts ~ 80 to 100 milliseconds, then dissolves. Wave packets form at rates of 2 to 7/second in all sensory areas, overlapping in space and time. Results of sensory information processing are seen in spatial patterns of amplitude modulation (AM) of wave packets with carrier waves in the gamma range (20 to 80 Hz in rabbits). The AM patterns correspond to categories of CSs that the rabbits can discriminate. The patterns are found in electroencephalographic (EEG) potentials generated by dendrites and recorded with high-density electrode arrays. The state transitions by which AM patterns form are manifested in the spatial pattern of phase modulation (PM), which have the radial symmetry of a cone. The apex of a PM cone marks the site of nucleation of an AM pattern. The phase gradient gives a soft boundary condition, where the axonal delay in spread gives sufficient phase dispersion to reach the half-power level. The size of the wave packets (10 to 30 mm in diameter in rabbits) is determined largely by the conduction velocities of intracortical axons through which the neural cooperation is maintained. The findings show that significant cortical activity takes the form of mesoscopic interactions of millions of neurons in broad areas of cortex, which are more clearly detected in graded dendritic potentials than in action potentials. The distinction is analogous to the difference between statistical mechanical and thermodynamic descriptions of particle behavior. Both types of neural activity show spatial and temporal discontinuities but at distinctive scales of microns and msec versus mm and tenths of a second. The aim of measurement here is to establish the wave packet as the information carrier at the mesoscopic level in brain dynamics, comparable to the role of the action potential as the information carrier at the microscopic level in neuron dynamics.

INTRODUCTION

Mapping of EEG local field potentials with high-density electrode arrays on sensory cortices has revealed high levels of local spatial coherence in the gamma range (20 to 80 Hz in rabbits). These episodes correspond to self-organized domains of neural activity that have been called 'wave packets' [Freeman 1975]. After band pass filtering the shared, broad-spectrum, chaotic wave form has been shown to maintain spatial distributions of amplitude modulation (AM). After training of subjects by reinforcement, spatial AM patterns emerge from the AM distributions. These AM patterns carried in wave packets are correlated with the categories of conditioned stimuli (CSs) that the animals have learned to discriminate [Freeman & Viana Di Prisco 1986; Freeman & van Dijk 1987; Freeman & Grajski 1987; Barrie, Freeman & Lenhart 1996; Ohl, Scheich & Freeman 2001]. These CS-related AM patterns have been identified in the olfactory bulb, prepyriform cortex, and the somatomotor, auditory and visual cortices (Figure 1). The problem addressed in this report is to measure the biological process of the chaotic dynamics by which these wave packets carrying AM patterns self-organize out of the on-going background AM distributions of gamma activity. The state transition has been simulated in elementary form in both software [Kozma & Freeman 2001] and VLSI hardware [Principe et al. 2001] embodiments, but omitting the propagation delays that are crucial determinants of the biological process.

Figure 1 near here

A key finding has been spatial patterns of phase modulation (PM) in wave packets that have radially symmetric gradients in EEGs from the olfactory bulb and sensory neocortices, but not in EEGs from the prepyriform cortex [Freeman & Barrie 2000]. These cones were first observed as an incidental finding in a study of AM patterns in gamma EEGs from the olfactory bulb [Freeman & Baird 1987]. The method then used for phase measurement was decomposition by nonlinear wavelets, for which the standard error of measurement (SEM) had been well documented [Freeman & Viana Di Prisco 1986]. Extension of this method to neocortical EEGs seemed prohibitively difficult, owing to the lack of markers in the form of distinctive alpha and theta waves, or temporal amplitude modulation of neocortical gamma activity in the form of 'bursts', by which to segment the EEGs. Fourier decomposition was used instead [Freeman & Barrie 2000] on overlapping segments of fixed length stepped at short intervals. The Fourier method succeeded in demonstrating the existence of phase cones in sensory neocortical EEGs, and it gave distributions by which to estimate their parameters of carrier frequencies, diameters, durations, phase gradients, transition velocities, and the spatial locations and signs of their apices.

The Fourier decomposition of each segment gave 50 phase cones, one for each frequency. There was no reason to suppose that these linear components represented any physiological variables. The determination of which one to use to characterize the segment might be either the best cone fit, the greatest spectral power, or the continuity with a previous location or frequency, but these were statistical criteria, not behavioral correlates. The phase cones were tracked to identify those which persisted at least as long as the phase cones in the bulb had lasted. The Fourier method applied to neocortical EEGs gave numerous overlapping cones with differing times of starting and ending. In contrast, the nonlinear basis functions applied to each bulbar burst following inhalation gave only two phase cones, both of which had the same time of onset, phase velocity, and location and sign of apices [Freeman & Baird 1987]. The distributions of neocortical parameters of phase cones differed in several other respects from those derived from bulbar EEGs. Most notably the bulbar cones had a fixed, hard boundary condition imposed by the anatomical extent of the bulb, whereas the neocortical cones had soft boundary conditions imposed by the phase gradients, which in turn were imposed by axonal transmission delays [Freeman 2000]. The bulbar transition velocities calculated from the phase gradients were not correlated with carrier frequency, whereas neocortical

transition velocities increased monotonically with the carrier frequency, and the neocortical half-power diameters varied without apparent correlation with carrier frequency.

A third method of phase measurement has been developed using the Hilbert transform [Freeman & Rogers 2002]. The analytic phase calculated from the 64 gamma EEGs has revealed a pattern of stable phase distributions that are sustained for tens to hundreds of msec, and that are punctuated by intermittent episodes of decoherence. The time series of the changes in phase differences between pairs of channels have given the appearance of a staircase pattern, in which the distribution of intervals between steps conformed to the durations and recurrence rates of the phase cones from the same data. The time derivative of the analytic phase sequences has shown spikes that occur in EEGs from different electrodes not simultaneously but over time intervals of 4-8 msec, corresponding to the phase gradients found in the cones. These data have given independent support to the inference that neocortical dynamics is characterized by sequential first order state transitions, that precede the formation of AM patterns.

The present study was undertaken to solve the problem of nonlinear wavelet decomposition of the neocortical EEGs, and to determine whether the differences in time series and parameters between bulbar and neocortical EEGs were due to methodological differences or were intrinsic to the two types of neuropil. The key to success lay in the result presented here that AM and PM patterns occurred intermittently, as had already been found for bulbar AM patterns, although the chaotic time series of EEG wave forms were continuous. This result led to the distinction [Freeman & Barrie 2000] between "AM patterns" in segments that could be classified with respect to behavior and "AM distributions" in segments that could not be so classified, and, further, to the inference that meaningful gamma patterns related to behavior were episodically embedded in continuous a flow of unpatterned gamma that has no behavioral correlates. The new results here confirm and extend the results from the Fourier and Hilbert transforms, provide narrower confidence intervals on the statistical assays of cone parameters, and give improved estimates of the temporal relations between AM and PM patterns. Together with previous findings the results help to establish the biological identity of the wave packet as a vector of mesoscopic information in the brain, which is carried by the microscopic action potentials not in the rates or frequencies of individual pulse trains but in the spatiotemporal organization of uncounted millions of neurons.

METHODS

The methods have been described for manufacture and surgical placement of arrays (Figure 1), maintenance and training of subjects, experimental design, and construction of data bases [Barrie et al. 1996], as well as techniques for preliminary temporal and spatial filtering of EEGs [Freeman & Viana Di Prisco 1986; Freeman & Baird 1987] and for classification of AM patterns of EEGs with respect to discriminative CSs [Freeman & Grajski 1987; Barrie et al. 1996]. Segments of EEGs simultaneously recorded from 64 electrodes in 8 x 8 arrays were measured by decomposing them with basis functions [Freeman 2000]. Measurement of amplitude was relatively precise [Freeman & Viana Di Prisco 1986], but measurement of phase was subject to large errors owing to the brief duration of segments, the small number of cycles in each segment, the strong tendency to frequency modulation (FM) and amplitude modulation (AM) about center frequencies and amplitudes in both time and space, and the mix of multiple frequencies in spectra of most segments, especially from neocortices with their tendency to "1/f²" spectra. The Fourier transform [Freeman & Barrie 2000] used linear basis functions to estimate the phase and amplitude of frequencies in the gamma range. The present study relied on nonlinear regression to fit wavelets [Freeman & Viana Di Prisco 1986], which were cosines linearly modulated in amplitude (AM) and frequency (FM) in time about center values. The sum of two wavelets was fitted to the each of the 64 EEG traces in segments lasting 64-128 msec, using the least mean square residuals as the criterion of convergence. The 2 wavelets were given by:

$$EEG_i(t) = \sum_{n=1}^2 v_{n,i} [1 + AM_{n,i}] \cos\{2 f_n [FM_{n,i}(t - t_m)] + \phi_{n,i}\} + r(t), i = 1, 64 \quad (1)$$

where t was the time base in the segment, $n = 1, 2$ was the number of the wavelet, $v_{n,i}$ was mean amplitude of the i -th component, $AM_{n,i}$ and $FM_{n,i}$ were fixed coefficients to represent linear amplitude and frequency modulation across the center of the time segment, t_m , f_n was the common center frequency of wavelet oscillation, $\phi_{n,i}$ was the desired phase of onset of the i -th damped cosine, and $r(t)$ was the residual after fitting the sum of the 2 wavelets to the EEG(t) segment. The sum was fitted by nonlinear regression [Freeman & Viana Di Prisco 1986; Chapter 2 in Freeman 2000] first to the spatial ensemble average EEG in order to estimate the common frequency, the AM and FM coefficients, and the reference phase, ϕ_n , after which the 64 phase values, $\phi_{n,i}$, and trace amplitudes, $v_{n,i}$, were estimated by fitting with nonlinear regression the same sum of two component cosines to each of the 64 traces, $i = 1, \dots, 64$, in which the phase for each channel and wavelet was calculated with respect to that of the ensemble average, ϕ_n . Thus each segment yielded four 8×8 matrices: one of amplitudes and one of phase for each of the two wavelets. The component with the largest amplitude was denoted "dominant", the other one "subsidiary".

The aim in using equation (1) was to derive optimal estimates of the phase of gamma oscillations for spatial pattern analysis. To that end the EEG data had to be pre-processed by band pass filtering. The high-amplitude, low-frequency component was removed for detrending up to 20 Hz by subtracting a cubic spline from each segment fitted by linear regression. The low-amplitude, high-frequency noise was removed with a step filter at 80 Hz. These parameters defining the gamma range were based on optimal classification of AM patterns with respect to behavior [Barrie et al. 1996]. Use of nonlinear regression required that initial guesses of nonlinear parameter values be supplied for the ϕ_n , f_n , $AM_{n,i}$ and $FM_{n,i}$ in order to initiate gradient descent. These were taken initially from mean values of preliminary assays from the same subject. After the first fit to the first segment of a trial set, the terminal values from the last preceding segment with successful fit were held over and used for each new segment. The 8×8 matrix of phase values for each wavelet and segment was smoothed with a 2-D spatial low pass filter set at 0.29 c/mm, previously optimized using the Fourier method [Freeman & Barrie 2000] by maximizing the % variance incorporated by fitting a cone to the EEG phase values.

The Standard Error of Measurement (SEM) was estimated by measuring a single cosine to which noise was added. The noise was provided by random numbers with zero mean and unit standard deviation, truncated as if by a 12 bit ADC, filtered in the same pass band as the EEG, and independently generated for 64 traces at zero phase adjusted to simulate the digitizing delay of 10 microseconds between channels. The amplitude of the cosine on different channels was varied to correspond to observed EEG amplitude distributions. The amplitude of the random number distributions was varied to give specified signal:noise ratios [Freeman & Viana Di Prisco 1986]. The method gave a scale by which to estimate the SEM of phase measurement, so that spatial and temporal EEG filters could be evaluated and optimized. The SEM averaged about $\pm 60^\circ$ for a single cosine fitted to raw EEGs. The SEM was reduced to $\pm 6^\circ$ after application to EEGs of the optimized wavelets in the form given by equation (1), the temporal filters specified above in pre-processing, & the spatial filter. The equations for the cones that were fitted to the 8×8 matrix of filtered phase values using nonlinear regression have been given [Freeman & Barrie 2000]. The three parameters were the location in mm of the apex in the two surface dimensions of the cortex under and around the array, and the slope (including sign) of the cone in radians/mm. The initial guesses were taken from the values determined in the last preceding segment successfully fitted.

Data were recorded from rabbits with 8 x 8 electrode arrays (0.79 mm spacing, 6 x 6 mm) fixed epidurally over the visual, auditory, or somatomotor cortex and trained to respond to discriminative CSs in the appropriate modality in a classical aversive conditioning paradigm with mild electric shock to the cheek as US and sniffing as CR. Each trial lasted 6 sec with a 3 sec control period preceding CS onset. Each subject in each training set was given 20 trials with a reinforced stimulus (CS+) and 20 trials with a non-reinforced stimulus (CS-) randomly interspersed. The search for significantly different, stimulus-induced, spatial AM patterns was conducted by stepping a fixed window along each trial record at over-lapping 16 msec time intervals. Each window having 64 EEG traces yielded a 64x1 column vector in amplitude. Forty trials yielded 20 CS- patterns and 20 CS+ patterns for each time step. Each pattern was normalized to zero mean and unit standard deviation to remove the global values of the AM patterns, which behavioral correlation had shown to be unrelated and detrimental to classification [Freeman & Viana Di Prisco 1986; Barrie et al. 1996]. The column vector then defined a point in 64-space. At each time step these patterns were further divided into two subgroups of 10 CS- patterns and two subgroups of 10 CS+ patterns. For one pair of subgroups of 10 each, denoted as training sets, the centers of gravity were calculated in 64-space. Classification of patterns as CS- or CS+ was determined by calculating the Euclidean distances of all patterns in the other pair of subgroups denoted as test sets. This procedure was repeated by cross-classifying all patterns in subgroups. A spatiotemporal pattern was classified correctly if the distance between that pattern and the centroid of its subgroup was less than the distance between the same pattern and the centroid of the opposite subgroup. The procedure was repeated at each time step to obtain a temporal sequence of the number of correctly discriminated spatiotemporal patterns within each window. The probability (p) that a number of patterns classified correctly with respect to the type of CS was significantly different from chance was determined on a binomial distribution probability scale. The values were plotted as time series. The classification assay was used to evaluate and optimize the search parameters for the phase cones. Full details concerning the assay including equations are to be found in Barrie et al. [1996].

RESULTS

1. Measurement of phase cones in relation to theta band activity

The EEG traces lasting 6 sec from up to 64 channels on each of 40 trials/session were segmented into overlapping windows 64-128 msec in duration and stepped at 2 msec intervals. Each segment was fitted by nonlinear regression to decompose the traces into the sum of the two nonlinear basis functions in equation (1) with the criterion of minimization of least squares residuals, (χ^2) . The initial guesses for the nonlinear parameters, frequency, f_n , and phase, ϕ_n , for the first segment of each session were taken from preliminary analyses of data from the same subject. For this analysis each of the 64 traces in each segment was band-pass filtered to give the gamma range (20-80 Hz in the rabbit) as previously found to be optimal for behavioral classification of spatial patterns of EEG amplitude [Barrie et al. 1996]. The spatial ensemble average was computed of the filtered segments (shown by the dots in the left frames of Figure 2). The FFT was computed to determine the peak frequency in the segment (dots in the right frames). The first wavelet at that frequency was computed with equation (1), fitted (light curves in left frames) and subtracted from the data (dots). The residuals (dark curves) were subjected to the FFT to determine their peak frequency (dark curves in right frames) in comparison to the FFT of the fitted wavelet (light curves). Its peak frequency was used to evaluate that of the second wavelet. These two frequencies were then fixed as initial guesses for nonlinear regression, and the phases and the amplitudes of the two wavelets were determined for all 64 traces in the segment. Thereafter the last preceding successful outcome was used to provide the initial guesses for each new segment.

Figure 2 near here

The four 8 x 8 matrices of amplitude and phase values from the two fitted wavelets were converted by Euler's formula to the real and imaginary parts, which were low-pass filtered spatially at 0.29 c/mm as previously described [Freeman & Barrie 2000]. The spatially filtered phase values were recovered by the inverse Euler operator and stored with the unfiltered values of amplitude. Each segment yielded four 8 x 8 matrices, the amplitude and phase of the dominant component (Figure 3) and those of the subsidiary component. On average across sessions and subjects the regression onto the EEG segments converged to less than 20% residuals in less than half the segments (Figure 4, **a**). The regression on 10 to 20% of the segments failed to converge at all ("100% residuals" in the figure), usually due to a singular matrix). These segments were omitted from further analysis. In convergent runs the "dominant" component wavelet captured typically >60% of the total variance of the EEG segment, while the "subsidiary" component wavelet caught ~20% of the variance. The middle frames of Figure 2 show the dominant wavelet and its spectrum when the residuals were <20% of the variance, corresponding to a trough in the plot in Figure 4, **a** and to >80% inclusion of the variance by the sum of the two basis functions. The phase values for each wavelet and segment were fitted using nonlinear regression with a cone (Figure 3, lower right frame), for which the initial guesses of the sign, slope, and location of the apex in 2-D came from the last preceding segment, giving two cones for each segment that were treated as separate entities. Failures of nonlinear regression were again encountered, but the regression on data in most segments converged with varying levels of residuals (Figure 4, **b**).

Figures 3 and 4 near here

The identification of long-lasting phase cones was undertaken as had previously been done with Fourier decomposition [Freeman & Barrie 2000] by searching for chains of segments in conformance with the following initial criteria: the sign of the apex was constant, the size of the step in location from each segment to the next was below 0.8 mm (the mean interelectrode distance), the cumulative drift across multiple segments from the site of first detection was below 1.6 mm, the frequency in Hz did not change more than 20 Hz in any one step, and the duration exceeded 76 msec (64 msec plus six 2 msec steps). These criteria were adapted by trial-and-error to individual subjects and sessions to give at least 2 cones but no more than 10 in the test period of every trial, resulting in a total of between 200 and 600 phase cones in 40 test periods from initial assay. An example of a raster plot of the temporal locations of the starting points of phase cones is shown in Figure 5 (**a**), in which each trial was represented by two lines. Starting points were plotted alternating on adjacent pairs of lines as a function of elapsed trial time in order to separate them visually on this long time scale. The duration of each short bar shows the number of time steps of 2 msec for which the phase cone was judged to be stable. Histograms of the phase cones over the sessions of 40 trials (Figure 5, **b**) showed equal numbers of phase cones in the control and test periods with no preferential increase in the number of cones at or just after CS onset.

Figure 5 near here

For each trial in a set of 40 trials the appearance of locations within trials of stable phase cones were represented as time series of step functions by assigning a value of unity to each digitized time within a cone and a value of zero to times between phase cones. The recurrence intervals appeared to correspond to fluctuations in the EEG in or below the theta range (3-7 Hz). In order to determine whether there was a statistical relation between the EEG and the appearance of phase cones the spatial ensemble average of the 64 unfiltered EEGs was calculated for each trial between 250 - 5750 msec (250 msec and been omitted at each end by the band pass filter used to extract the phase cones). The spatial averaging of course attenuated the gamma activity with its phase dispersions but largely retained the low frequency activity. The autocovariances of the phase cone appearances and unfiltered EEGs and their crosscovariance were calculated across the 40 trials with the shift in both directions ± 1250 bins (± 2500 msec) to avoid end effects between trials. The

Fourier transform was applied to the autocovariances and crosscovariance to get the real and imaginary parts of the power spectra. The averages of these parts over trials served to give the mean amplitude (square root of the power) and cross-spectra for the phase cones (Figure 6, **a** and **b**, upper frames) and the unfiltered EEGs (middle frames). In about half the subjects there was a peak for the EEGs in or below the theta range (Figure 6, **a**) but not in the other half (**b**), irrespective of the type of cortex (visual, auditory or somatomotor). In all subjects there was a corresponding peak in the cross-spectrum between the time series of the appearance of the phase cones and the spatial average of the unfiltered EEG (lower frames). No significant differences were found in this property between cortices.

Figure 6 near here

2. Description of properties of phase cones

The peak in or below the theta range of the cross-spectrum provided a criterion for optimization of the parameters used for the detection and measurement of phase cones. Three representative sets of data values are shown in each frame of Figure 7 documenting the search for maximal values of the theta-band peak of covariance by varying (**a**) the minimal value of % residuals in fitting wavelets to the EEGs, (**b**) the minimal value of % residuals on fitting the cone to the phase data, (**c**) the choice of minimal duration of phase cones, and (**d**) the maximal range of drift allowed before cut-off. The sets of values for the optimized search parameters from 9 sessions with 3 subjects are shown in Table 1, together with the optimal minimal cone diameter.

Figure 7 and Table 1 near here

The recurrence rates were expressed by the number of phase cones found in the test periods after the onset of the CS and before the trial ending. Table 2 shows the predicted numbers derived from the peak frequency in or near the theta band and the averages of the observed numbers in the 9 subjects. Although the averages across all subjects were similar, there were 2-fold disagreements among the estimates in both directions in individual subjects. These differences were accompanied by wide variations in the numbers of cones over trials and in the intervals between cones as exemplified in Figure 5. No specific source for the discrepancies has been found.

Tables 2 and 3 near here

Table 3 gives the modes and 95% upper limits from the 9 subjects. Examples of the distributions of the quantities of main interest are shown in Figure 8: (**a**) the % residuals of the cone fit, (**b**) the transition velocities in m/sec, (**c**) the carrier frequencies in Hz, (**d**) the half-power diameters in mm, (**e**) the phase gradients in radians/mm, and (**f**) the step sizes in mm within stable cones. These statistics were compiled from phase cones above the minimal fit in the EEG regression, above the minimal duration, and below the maximal allowed drift but without truncation by carrier frequency, cone % residual or cone diameter. Segments for which nonlinear regression returned % residuals above the optimal level or diameters less than optimal were thereafter dropped. Segments having carrier frequencies outside the gamma range were also dropped, because the focus of this study was on the gamma range as defined for a species by the classification of AM patterns with respect to behavior above a specified level of significance [Barrie et al. 1996]. Distributions of carrier frequencies were often nearly normal but as often skewed to the lower frequencies having higher amplitudes in the gamma range in accordance with the " $1/f^2$ " spectral power distribution. The distributions of the phase gradients were always bimodal, usually with a 2:1 preponderance of negative values (phase lag at the apex). Distributions of durations, velocities and diameters were always skewed to lower values.

Figure 8 near here

Previous results from the olfactory bulb had yielded estimates of transition velocity that did not depend on carrier frequency. The data from neocortical EEGs showed that carrier frequency, transmission velocity, half-power diameter all increased together monotonically (Figure 9). The ordinary correlation coefficients were all positive (see legend). So were the partial correlations between velocity and diameter, and between velocity and frequency, but the partial correlation between frequency and diameter was negative. This result was consistent with the prior finding in these neocortical data of noncorrelation of diameter with respect to carrier frequency [Freeman & Barrie 2000].

Figure 9 near here

A comparison was undertaken of the phase cones derived from the dominant and subsidiary wavelets fitted to each segment. In previous results from the olfactory bulb [Freeman & Baird 1987] the two carrier frequencies differed on average by ± 19 Hz, the signs of the 2 apices (lead or lag) were always the same, and the locations of the apices were sufficiently close that the standard error was about half the interelectrode distance that gave the spatial grain of measurement. Bulbar gradients in radians/mm varied inversely with frequency and converged to closely similar estimates of transition velocity (dominant 1.72 ± 0.39 m/sec; subsidiary 1.87 ± 0.47). In the present results (Figure 10) from the neocortical EEGs the modal differences (c) in carrier frequencies (a and b) were ± 22 Hz, again with a preponderance of lower frequencies in the dominant component, and the modal transition velocities differed (dominant 3.01 ± 1.21 m/sec; subsidiary 4.52 ± 1.83 m/sec). However, the signs of the apices failed to agree in about half the subjects, so that the distributions of the differences between gradients (d and e) were trimodal (f) and centered at zero radians/mm. The variation in the locations between each pair of apices within stable cones (Figure 11, a) was close to that for the locations between successive dominant cones (b). The modal distances between apices of successive stable cones were 20-fold greater than the drift within stable cones (Figure 8, f), one-third of the modal half-power diameter, and one-seventh of the 95% level of half-power diameter (Table 3).

Figures 10 and 11 near here

3. Relation of spatial phase modulation (PM, phase cones) to spatial amplitude modulation (AM patterns)

Gamma bursts and theta waves in olfactory EEGs facilitated finding relations between spatial AM and PM (phase modulation) patterns owing to fluctuations of sensory receptor input with the respiratory cycle, which caused temporal amplitude modulation ("bursts") in the gamma band and a prominent respiratory wave in the theta band. Comparable temporal AM patterns were not apparent in the neocortical EEGs, though evidence had been found in these data for the recurrence of spatial AM patterns [Barrie et al. 1996] and spatial PM patterns (cones, Freeman & Barrie 2000] at rates in and below the theta range. In previous studies the neocortical spatial AM distributions were measured by calculating the root mean square (RMS) amplitudes in fixed windows usually lasting 64 msec and overlapped in steps optimally of 16 msec with the same fixed time reference on all trials at the start of CS onset (3000 msec). The locked step AM distributions were explored to find EEG segments with AM patterns (distributions related to CSs) by classifying them across 40 trials, 20 with CS+ and 20 with CS-. The more likely locations of the AM patterns in time across trials were given by a high probability of correct classification of the AM distributions with respect to the CSs [Barrie et al. 1996]. The same methods of RMS calculation, locked step segmentation, and classification were here applied to the AM distributions measured by wavelet amplitudes.

Examples of the results in the upper frames of Figures 12, 13 and 14, 'Locked steps (a)' show that correct classification did not occur before CS arrival, and it occurred if at all most clearly just after CS arrival but less reliably thereafter.

Figures 12 - 14 near here

A likely factor in the reduced classification later in test periods was an intertrial variation in times of onset of the AM patterns of gamma activity termed "jitter" by Tallon-Baudry et al. [1998]. An alternative strategy was therefore devised to select segments containing AM distributions for classification by using the information about the locations of phase cones, on the assumption that the PM patterns marked the state transitions by which the AM patterns were formed. The search was instituted with the data base of 165 AM patterns from 64 msec in 16 msec steps in the 2640 msec starting at 3000 msec and running through 5640 msec. At each time point a search was made on every trial for the starting point of the nearest phase cone before or after the time of beginning the search. Then the AM segment nearest that phase cone was substituted for the AM segment at that step on every trial. This procedure did not use the previously determined start times of the phase cones, but instead brought in the pre-calculated RMS distribution in the 64 msec segment nearest the phase cones. It re-used the same cones and AM distributions in multiple steps, which further reduced the temporal resolution of the classification of AM patterns with respect to behavior. With this modification the peak in classification just after CS onset was reduced, and two or more peaks of classification were increased later in the test periods, as exemplified in the lower frames of Figures 12 to 14, 'Use phase cones (b)'. The numbers and locations in time of the peaks varied across subjects without notable differences assignable to the three neocortices.

The data base from 40 trials of each subject had a rigid temporal framework. On each trial 165 AM distributions were calculated from segments lasting 64 msec stepped at 16 msec intervals and stored for retrieval by indexing. In order to surmount the rigidity of this framework and investigate the temporal relations between AM and PM patterns, the entire RMS data base was shifted with respect to the data base of starting and ending times of the phase cones on the 40 trials in steps of 8 bins (64 msec) over a range of ± 16 steps (± 256 msec). The classification was repeated at each step. An assay of the over-all goodness of classification was provided by counting the number of steps out of 165 in which the number of correctly classified patterns was 26 or greater ($p < .05$). The over-all assay varied substantially with this procedure, as shown by the examples in Figure 15, which enabled the selection of an optimal shift value giving the highest level of EEG classification with respect to behavior for each session and subject, as shown Table 2 in msec (right-most column). These shift values were compared with the time shifts from the cross-spectra of the spatial ensemble averages of the EEGs vs. phase cones (adjacent column), using the peak frequency to convert the phase values to time lags in msec (Figure 16). The correlation coefficient between the 9 pairs of time shifts was 0.82. The two estimates in Table 2 of average time lead the phase cone onset before the AM pattern onset were $+31 \pm 28$ (SE) msec and $+34 \pm 31$ (SE) msec.

Figures 15 and 16 near here

The relations between AM and PM patterns were further evaluated by setting up a third data base containing the RMS amplitudes within the time frames specified by the starting and ending of the phase cones. During the set-up for a classification over trials at each step, instead of the nearest fixed-duration, fixed step AM distributions being used, the RMS distributions of the nearest phase cone epochs were calculated in the time frames designated by start and end. This substitution had little or no effect on the classification levels, but it allowed shifting of the time of onset of the calculation of each RMS pattern with respect to the time of onset of its phase cone. This was done by extending or delaying the start of the time base for calculation of the RMS segment earlier or

later than the time of onset of the phase cone in steps of 2 bins (4 msec) while keeping the end point constant. The classification rate was assayed by the same technique as that for Figure 15. The same procedure was next done while fixing the start times at the optimized values and varying the RMS end points in 4 msec steps before and after the ending of the phase cones. Two examples of the effect of applying this algorithm before the classification assay are shown in Figure 17 for start times (**a**) and end times (**b**). The mean optimal lag in starting time of the RMS patterns from the start of the phase cones was 24 ± 20 (SE) msec, which was above zero lag by the SE of the mean and within the SEs of the two other estimates (Table 2). The mean optimal lag in ending time from the ends of the phase cones was 5 ± 8 (SE) msec, indicating no significant difference in ending times of the AM and PM patterns. Combining the three estimates of onset delay gave 30 ± 5 (SE) msec for the average time delay from the start of a phase cone to the establishment of an AM pattern, about 1.5 cycles at the modal gamma carrier frequency.

Figure 17 near here

DISCUSSION

The main problem encountered in attempting decomposition of neocortical EEGs with the type of wavelet that had succeeded with olfactory EEGs was the prohibitively high incidence of poor fits and outright failures of nonlinear regression to converge to a solution. Close tracking of performance brought to light the intermittency of successful convergence, which in turn led to recognition that segments amenable to wavelet decomposition were to be found in the gamma band of neocortical EEGs at about the same rates and durations as respiratory-related 'bursts' in olfactory EEGs. The successfully decomposed segments appeared to be separated by "junk" gamma which appeared to be comparable to the interburst "noise" in the bulbar EEGs, for which wavelet decomposition did not succeed. About half of the remaining segments could be fitted with a symmetrical conic surface with better than 80% inclusion of the variance by the cone.

Although the intervals between putative phase cones had suggested mean recurrence rates in the alpha and theta ranges [Freeman & Barrie 2000], the intervals were highly variable, and visual inspection of sets of EEGs with no filtering beyond that during recording (analog pass band 0.1 to 100 Hz) seldom revealed episodic periodicity in the theta and alpha ranges. The spectrum of the autocovariance of the EEG often failed to show an amplitude peak accompanying the peak in the cross-spectrum between the EEG and the phase cones, reflecting the common lack of appearance of near-periodic theta waves in time series displays of the EEGs despite the high level of energy distributed in that part of the spectrum, much of it apparently unrelated to phase cones. Calculation of autocovariance and crosscovariance over the entire set of 40 spatial ensemble averages was required. The resulting peak in the cross-spectrum in or below the theta range provided a useful assay by which to evaluate and optimize the several parameters that were necessary for identification of stable phase cones. Each parameter was varied over suitable steps in an appropriate range to construct a tuning curve, by which the maximum of covariance could serve to indicate the optimal value of the parameter. The results gave estimates in terms of minimum, mode, and 95% upper inclusion level of the values of the main properties needed to describe phase cones: duration, recurrence rate, location of the apex, spatial distance between sequential cones, phase gradient, transition velocity, carrier frequency, and half-power diameter. Most remarkable were the sizes of the wave packets (Figure 1), which were large enough to most if not all of the multiple subsidiary regions into which each primary sensory area has been parceled in different species. The implication in regard to spatial integration of sensory-driven neural activity into gamma oscillations prior to perception is obvious.

Support for the validity of the parameter estimates was provided by the strong positive ordinary correlations between velocity and diameter, and between velocity and frequency, but a negative

partial correlation between frequency and diameter. A high velocity would imply large diameters of axons that served to carry out the underlying state transition, and those axons might lead to a high carrier frequency by rapidly initiating the widespread cooperative activity needed to generate the carrier wave. However, owing to increased phase dispersion with propagation delays a high frequency would have worked against maintaining a large diameter of cooperative activity, giving the observed negative partial correlation. Additional support for the validity was given by the convergence of three independent measures of the time relationships between the onsets of phase cones and the onsets of the AM patterns, all indicating that cones lead the formation of AM patterns, and that both on average terminate together. In terms of the life cycle of a wave packet described by its AM and PM patterns, given the $\pm 95\%$ range of carrier frequencies (32-82 Hz) about the mode (48 Hz), the estimated time required for the state transition to establish a wave packet to its half-power diameter is 5.2 ± 2.2 msec. The combined three measures of AM delay give an estimate of 30 ± 5 msec, about 1.5 cycles, for the time needed after a cortical state transition for a new AM pattern to form. The range of duration, 79-101 msec, suggests that the oscillation fades after 4-5 cycles at the modal carrier frequency, and that 100-400 msec then elapses before the next state transition. These data together with the results from the analytic phase [Freeman & Rogers 2002] support the inference that formation of AM patterns is by a first order state transition that is comparable to the physical transition from a gas to a liquid. The "binding" of information provided by sensory "feature detectors" is more akin to the condensation of particles from a disorganized state to a more interactive state, than to the linear summation of neural pulse trains to zero phase lag at a single frequency [Singer & Gray 1995].

Both bulbar and neocortical EEGs under wavelet decomposition yielded pairs of overlapping cones, but with the difference that the bulbar dominant and subsidiary cones always had the same sign and location of the apices and transition velocities, whereas the pairs of wavelets from neocortical EEGs showed that coexisting cones had independent signs and locations of apices. This evidence suggests that areas of neocortex can sustain more than one cooperative domain simultaneously in some form of multi-tasking. Such proposed 'time-sharing' is fully compatible with the low demands for covariance of each cooperative domain on the total variance sustained by background activities of interacting cortical neurons [Freeman 2000] on the order of 0.1% to 1%..

Another difference between bulbar and neocortical cones derived with wavelets was in the distributions of the gradients. Whereas the signs of the apices were equally distributed between extremes of lead and lag in the bulbar data and also in the neocortical EEG data upon Fourier decomposition, in the present data there was a preponderance of phase lag, often by a ratio of 2:1 over phase lead at the apex. There is no explanation of the asymmetry. Another unexplained fact: in neocortical data by both Fourier and wavelet decomposition there was a predominance of phase cones with durations shorter than the minimum derived here by optimization of the amplitude of the peak of the cross-spectra in or below the theta range. Histograms of the distributions of cone durations without screening for minimal duration showed that the mode was at or just above the 2 msec digitizing interval. It is unclear whether these short-lasting cones are statistical flukes, abortive cones, or an indication of some as yet unknown short-comings in the techniques for extracting cones from the EEG data.

The most difficult aspect of the analysis of phase cones concerned the relations of the cones to AM patterns and to behavior. A notable discrepancy between the results from Fourier and wavelet methods was the absence of a significant increase in numbers of phase cones at the times of CS arrivals in cortex, and the decline in the CS+/- classification index in the 250-300 msec time interval following CS onsets, when the selection of segments was based on phase cones. This finding suggests that the impact of an afferent volley on a sensory neocortex forces a pattern of cortical activity that can be identified through CS-specific AM patterns, but one which is not endogenously self-organized and therefore has no accompanying state transition or phase cone.

This inference is compatible with results of spatial analysis of the EEGs from the auditory neocortex in the Mongolian gerbil [Ohl, Scheich & Freeman 2000, 2001], in which stimulus-specific tonotopically organized patterns were found in the first 250 msec after CS onset, and endogenous global patterns constituting generalization and abstraction were found thereafter. Alternatively, the absence of the peak in correct classification upon stimulus arrival might be ascribed to the method used here in which the nearest phase cones were selected from both before and after CS onset.

Future studies in animals might usefully be directed toward an evaluation of the utility and significance of the matrices of the FM and AM coefficients from wavelet decomposition by equation (1); search for the phase interrelations of EEGs simultaneously recorded from multiple neocortices and the olfactory system; mapping the cumulative cortical areas covered by repeated phase cones with their varying diameters and apical locations; and search for inputs to neocortices comparable to the recurrent driving of the bulb by respiration, which constitutes a forcing function, the sniff, that might have its counterpart in the visual saccade, finger tremor, and gating of auditory input at frame rates in the infrasonic (subaudible) by the muscles of the middle ear under efferent control. In addition to Fourier and wavelet methods the calculation of the analytic phase by the Hilbert transform should be applied to these EEGs, in the light of the high temporal resolution provided by this operator [Tass et al. 1999; Freeman & Rogers 2002].

Although not tested in the present study, previous analyses of bulbar and neocortical phase cones [Freeman & Baird 1987; Freeman & Barrie 2000] have provided strong evidence that the locations of phase cones are not related to CSs. If in accord with the nonlinear dynamic theory applied to cortex each AM pattern must be preceded by a state transition and carry the imprint of the transition in a phase cone, then the cone should serve as the best available indicator to date of where and when to find the AM patterns embedded in the otherwise featureless "junk" gamma, whatever its cognitive content. The main obstacle to further improvements in search of more complex behavioral correlates of gamma activity appears to lie not so much in the techniques of EEG analysis as in the richness of the inner dynamics of the subjects that is indicated by the high recurrence rates of phase cones both before and after CS onsets, presently without identified AM patterns. Whatever is going on in the subjects' brains, it is undoubtedly much more than the simple information processing that is required to deliver conditioned responses on cue. Significant progress in this direction may await application of spatial phase analysis to intracranial EEGs in primates [Freeman & van Dijk 1987] and human EEGs in studies of the behavioral correlates of gamma activity recorded on the scalp [Müller et al. 1996; Tallon-Baudry et al. 1998; Freeman et al. 2000].

ACKNOWLEDGMENTS

This study was supported by a grant MH06686 from the National Institute of Mental Health and by a grant EIA-0130352 from the National Science Foundation to R. Kozma. The contributions of John Barrie and Mark Lenhart to the data acquisition have been recognized in prior publications. Special appreciation is due to Brian C. Burke for his skills in system and program development, precision testing of software, and reliable management of immense data bases, without which the present analyses could not have been done.

REFERENCES

- Barrie, J.M., Freeman, W.J. & Lenhart, M.D. [1996] Spatiotemporal analysis of prepyriform, visual, auditory and somesthetic surface EEGs in trained rabbits. *J. Neurophysiol.* **76**: 520-539.
- Freeman, W.J. [1975] *Mass Action in the Nervous System*. New York: Academic Press.

- Freeman, W. J. [2000] *Neurodynamics. An Exploration of Mesoscopic Brain Dynamics*. London UK: Springer-Verlag.
- Freeman WJ [2000] Characteristics of the synchronization of brain activity imposed by finite conduction velocities of axons. *Int. J. Bifurcation & Chaos* **10**: 2307-2322.
- Freeman, W.J. & Baird, B. [1987] Relation of olfactory EEG to behavior: Spatial analysis. *Behav. Neurosci.* **101**: 393-408.
- Freeman, W.J. & Barrie, J.M. [2000] Analysis of spatial patterns of phase in neocortical gamma EEGs in rabbit. *J. Neurophysiol.* **84**: 1266-1278.
- Freeman, W.J. & Grajski, K.A. [1987] Relation of olfactory EEG to behavior: Factor analysis: *Behav. Neurosci.* **101**: 766-777.
- Freeman, W.J. & Rogers, L.J. [2002] Fine temporal resolution of analytic phase reveals episodic synchronization by state transitions in gamma EEGs. *J. Neurophysiol.* in press (Feb).
- Freeman, W.J., Rogers, L.J., Holmes, M.D. & Silbergeld, D.L. [2000] Spatial spectral analysis of human electrocorticograms including the alpha and gamma bands. *J. Neurosci. Methods* **95**: 111-121.
- Freeman, W.J. & van Dijk, B. [1987] Spatial patterns of visual cortical fast EEG during conditioned reflex in a rhesus monkey. *Brain Research* **422**: 267-276.
- Freeman, W.J. & Viana Di Prisco, G. [1986] Relation of olfactory EEG to behavior: Time series analysis. *Behav. Neurosci.* **100**: 753-763.
- Kozma R, & Freeman, W.J. [2001] Chaotic resonance: Methods and applications for robust classification of noisy and variable patterns. *Int. J. Bifurcation & Chaos* **11**: 1687-1729.
- Müller, M.M., Bosch, J., Elbert, T., Kreiter, A., Valdes Sosa, M., Valdes Sosa, P. & Rockstroh, B. [1996] Visually induced gamma band responses in human EEG - A link to animal studies. *Exper. Brain Res.* **112**: 96-112.
- Ohl, F.W., Scheich, H. & Freeman, W.J. [2000] Topographic analysis of epidural pure-tone-evoked potentials in gerbil auditory cortex. *J. Neurophysiol.* **83**: 3123-3132.
- Ohl, F.W., Scheich, H. & Freeman, W.J. [2001] Change in pattern of ongoing cortical activity with auditory category learning. *Nature* **412**: 733-736.
- Principe, J.C., Tavares, V.G., Harris, J.G. & Freeman, W.J. [2001] Design and implementation of a biologically realistic olfactory cortex in analog VLSI. *Proc. IEEE* **89**: 1030-1051.
- Singer, W. & Gray, C.M. [1995] Visual feature integration and the temporal correlation hypothesis. *Ann. Rev. Neurosci.* **18**: 555-586.
- Tallon-Baudry, C., Bertrand, O., Perronet, F. & Pernier, J. [1998] Induced γ -band activity during the delay of a visual short-term memory task in humans. *J. Neurosci.* **18**: 4144-4154.
- Tass, P, Kurths, J, Rosenblum M, Weule J, Pikovsky A, Volkmann J, Schnitzler H, Freund, H. [1999] Complex phase synchronization in neurophysiological data. In: *Analysis of Neurophysiological Brain Functioning*, (ed. Uhl, C.), Berlin: Springer, pp. 252-273.

Tables

type of cortex	min EEG % var.	min cone % var.	min dur msec	min diam mm	max drift mm
VC	85.0	72.5	76	7.5	0.9
VC	87.5	77.5	76	7.5	1.4
AC	87.5	77.5	76	10.0	1.4
AC	97.5	72.5	76	10.0	0.9
AC	97.5	85.0	80	10.0	1.1
AC	92.5	75.0	76	10.0	0.8
SC	90.0	70.0	72	7.5	0.8
SC	82.5	77.5	72	7.5	1.0
SC	87.5	75.0	76	7.5	1.3
average	88.6	75.8	75.6	8.6	1.06
SD	4.4	4.3	2.4	1.3	0.24

Table 1. The values are shown of the criteria for identification of stable phase cones after optimization of the amplitude of the peaks in covariance between the appearance of the phase cones and the spatial ensemble average across the 64 electrodes of the unfiltered EEGs in or below the theta range, including minimal % variance included by the wavelets, minimal % variance included by the phase cones, minimal duration and diameter of the cones, and maximal drift from the point of first identification. No significant differences were found between results from visual (VC), auditory (AC) and somatomotor (SC) cortices.

type of cortex	coherence peak	frequency Hz	phase radians	predicted #/trial	observed #/trial	cone lead msec	opt shift msec
VC	0.89	4.52	-2.44	10.8	5.8	86	48
VC	0.44	2.32	2.79	5.8	5.2	-77	16
AC	0.58	3.3	-1.39	7.9	4.6	77	96
AC	0.80	4.88	1.67	11.7	6.9	-54	-144
AC	0.55	6.35	0.28	15.2	17.5	-7	0
AC	1.10	4.52	0.45	10.8	4.2	-31	-16
SC	0.44	5.74	-0.37	13.8	15.9	18	0
SC	0.36	2.81	-2.36	6.8	13.3	181	128
SC	0.88	2.08	-2.37	5	11.1	83	176
average	0.67	4.02	-0.42	9.7	9.4	31	34
SD	0.25	1.53	1.89	3.6	4.9	83	93

Table 2. A comparison is made between the number of cones predicted in the test period (3000 to 5640 msec) of each trial from the frequency of the peak of covariance in or near the theta range and the number observed in the total of 40 trials. The rate of change in the phase cross-spectrum with respect to frequency was extremely high (e.g., ~1 radian for each increment of 0.06 Hz) in the region of the covariance peaks, so the method gave a very wide confidence interval for the values of phase at the peaks. Cone lead was taken from the phase cross-spectrum. For optimal shifts see Figures 15 and 16.

type of cortex	frequency Hz	velocity m/sec	upper 95% m/sec	diameter mm	upper 95% mm	distance mm	upper 95% mm	duration msec
VC	37	1.9	6.1	13	19	4.5	19	105
VC	42	2.1	9.8	12	22	3.1	12	106
AC	39	1.9	7.7	12	31	3.8	23	101
AC	42	2.4	7.9	14	24	3.9	13	99
AC	61	3.8	9	16	28	4.3	9	98
AC	68	5.2	7.5	19	26	2.2	33	104
SC	52	4.2	8.2	20	38	2.9	14	92
SC	40	2.2	6.9	14	23	2.5	15	101
SC	50	3.7	8.3	18	41	4.2	14	102
average	47.9	3.04	7.9	15.3	28	3.5	17	101
SD	10.8	1.21	1.1	3.04	7.4	0.8	7.3	4.3

Table 3. Values for all subjects are listed for the modes and upper 95% levels of the distributions of the center frequency in Hz of the dominant wavelet (that having the higher amplitude) fitted to the segments in the moving window, the phase transition velocity in m/sec, the half-power diameter of the phase cones, and the distance between apices of successive cones, as well as the upper 95% bound of the duration of phase cones. The lower bounds of duration (75.6 ± 2.4 msec) and diameter (8.6 ± 1.3 mm) were set by covariance optimization (see Figure 7, Table 1).

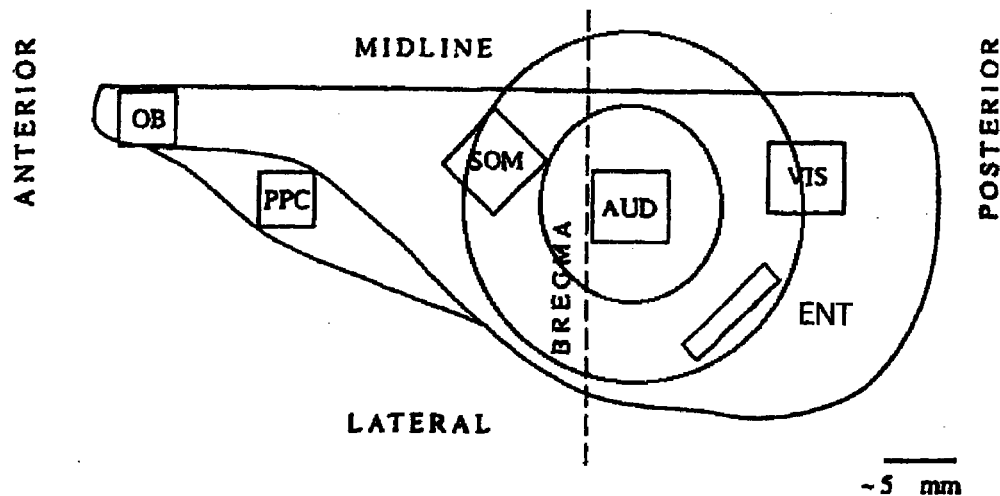


Figure 1. The left cerebral hemisphere of the rabbit brain is shown as seen from above. The rectangles show the locations of the 6x6 mm (8x8 electrode) arrays. The circles show the size of phase cones ("condensation rings") that result in wave packets. The inner circle shows the modal diameter of 15 mm. The outer circle shows the 95% inclusion diameter of 28 mm. The wave packets manifested by phase cones are far larger than the sizes of cortical columns and hypercolumns, covering the whole extent of each sensory cortex, including the multiple topographic maps for selected stimulus features. The wave packet is a candidate for the neural mechanism by which the information that is sent to cortex by sensory receptors is integrated into percepts shaped by past learning embedded in modified intracortical synapses.

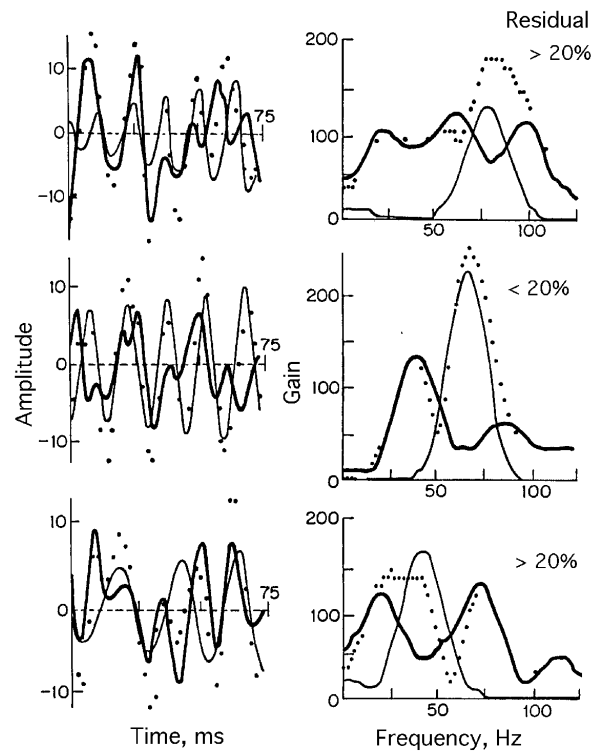


Figure 2. The technique is illustrated for fitting wavelets (light traces in left frames) to short segments of band-pass filtered EEGs digitized at 2 msec (dots) using the FFT to estimate the center frequencies of the wavelets. The linear temporal amplitude and frequency modulation of the wavelets is apparent as determined by equation (1). The residuals fell below 20% (middle frame) when a dominant spectral peak appeared (see Figure 4).

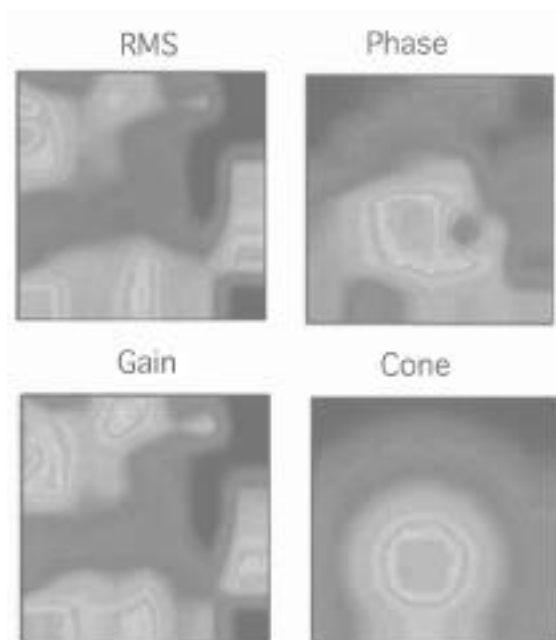


Figure 3. In a representative segment the gains (lower left) of the dominant wavelet from nonlinear regression of the two wavelets from equation (1) onto the 64 traces are shown by a contour plot (red is maximal amplitude) in comparison with the root mean square (RMS) amplitude (upper left). The phases of the 64 traces displayed in a contour plot (upper right where red is maximal phase lead) are compared with the form of the fitted cone (lower right). [original in color]

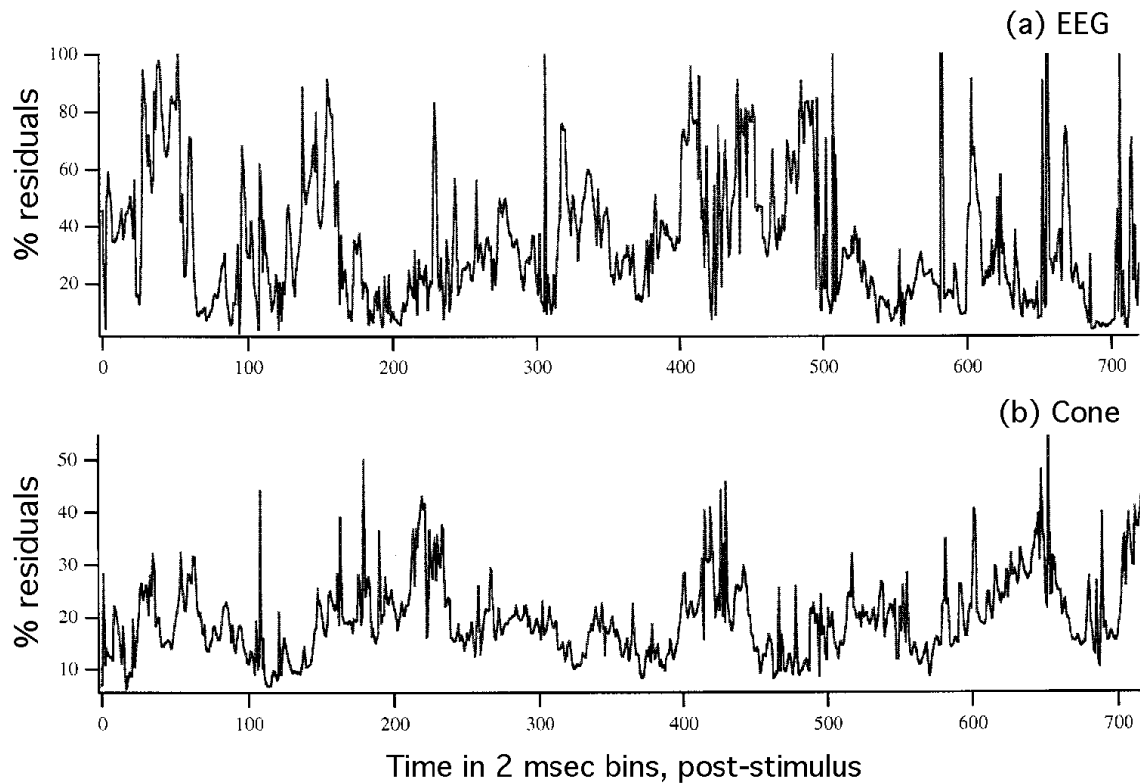


Figure 4, a. An example is shown of the % residuals after optimization by nonlinear regression of the fitted sum of 2 nonlinear wavelets (AM and FM cosines given by equation (1)) to the 64 EEGs in a moving window of 64 msec stepped at 2 msec. The EEGs were band pass filtered (20-80 Hz) giving traces 5280 msec in length. The values are shown from the first 1440 msec post-stimulus. Failure of the regression to converge is shown by the peaks at 100% residuals.

b. An example is shown of the % residuals after optimization of the fit of a cone to the spatially filtered 8 x 8 matrix of phase values (see Figure 3). Optimized thresholds are given in Table 1.

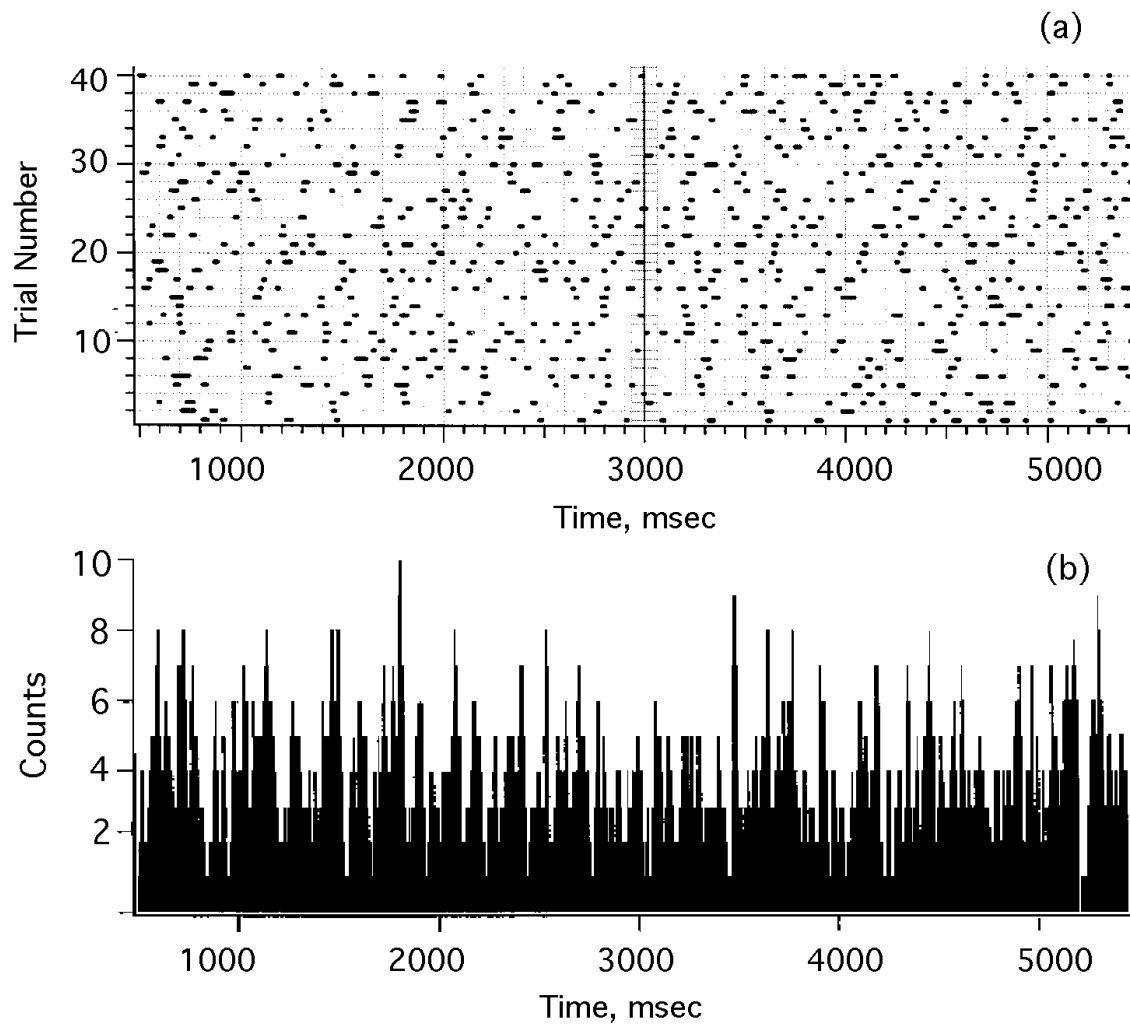


Figure 5. a. An example is shown from the visual cortex of the temporal locations of the starting times of the appearance of stable phase cones in a set of 40 trials. The duration of each bar indicates the number of steps over which the phase cones was followed; the actual duration would be indicated by adding 32 bins (64 msec) to each bar. This type of data was used to describe the appearance of phase cones in a session as a time series of step functions.

b. A histogram of the times of onset shows no preferential increase at or immediately after the time of stimulus onset (3000 msec).

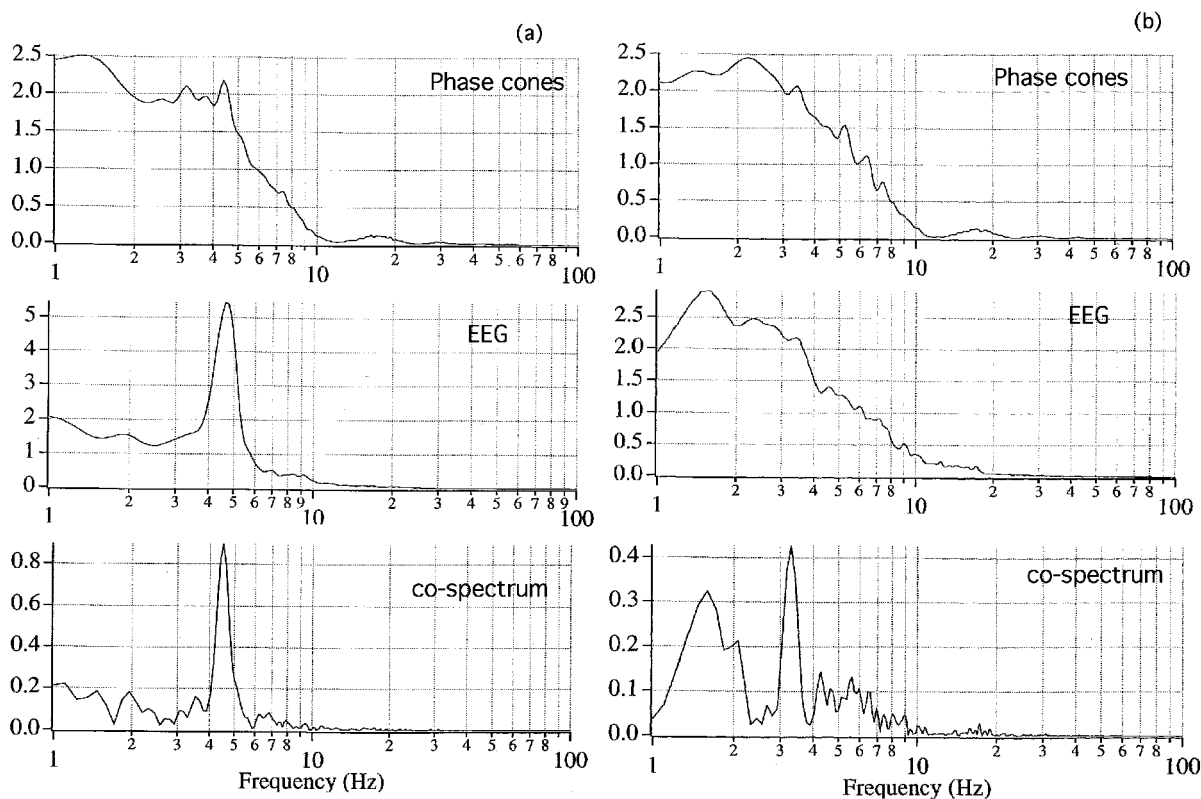


Figure 6. The amplitude (square root of power) spectra and cross-spectrum of the autocovariances and crosscovariance of the phase cone appearances and the unfiltered EEG (the spatial average over the same 64 traces that were used to determine the phase cones) were plotted as a function of log frequency. The cones were derived from EEGs temporally and spatially filtered to extract the gamma activity. The spectra of the EEGs without gamma band filtering (only analog, 1-100 Hz), when plotted in log-log coordinates (Barrie, Freeman and Lenhart 1996; Freeman and Barrie 2000) revealed their typical " $1/f^2$ " form.

- a. This example from the auditory cortex shows prominent theta peaks in the EEG, phase cones and cross-spectrum.
- b. The example from visual cortex showed little or no theta peak in the EEG or phase cone appearances but a clear peak in the cross-spectrum.

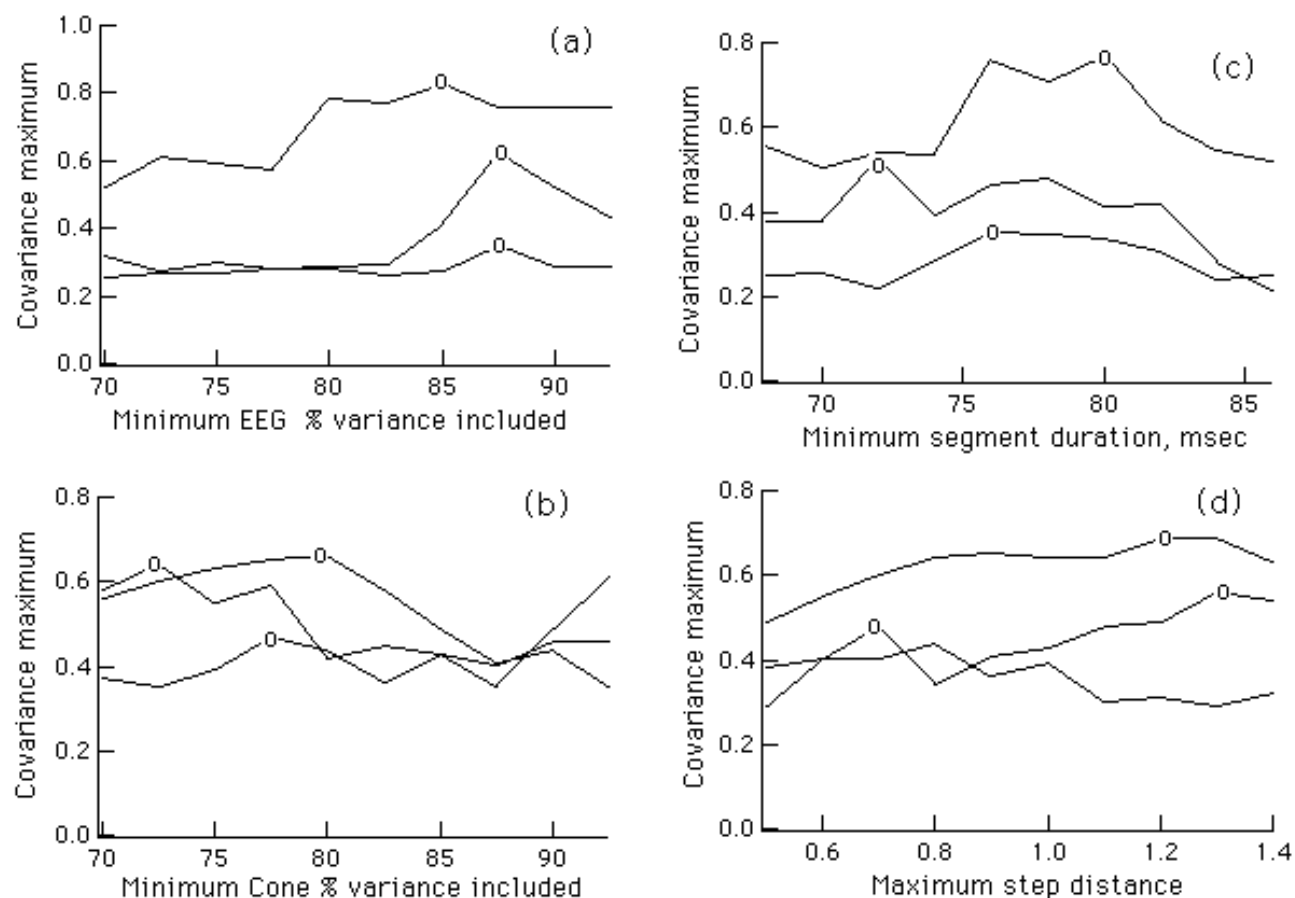


Figure 7. Three examples are shown of the search through the parameter space of long-lasting stable phase cones by maximizing the covariance amplitude in the cross-spectrum between EEGs and phase cones. Optimal values are indicated by the symbol "o".

- a.** Minimal % variance included in the nonlinear regression of wavelets on the EEGs.
- b.** Minimal % variance included in the nonlinear regression of cones on the phase data.
- c.** Minimal segment time duration in msec.
- d.** Maximal drift distance in mm (largest distance from site of initial identification but still within the same phase cone by other criteria).

The optimized values for the 9 subjects are shown in Table 1. Changes in individual parameters showed relative insensitivity but cumulatively gave notable increase in the frequency-specific covariance.

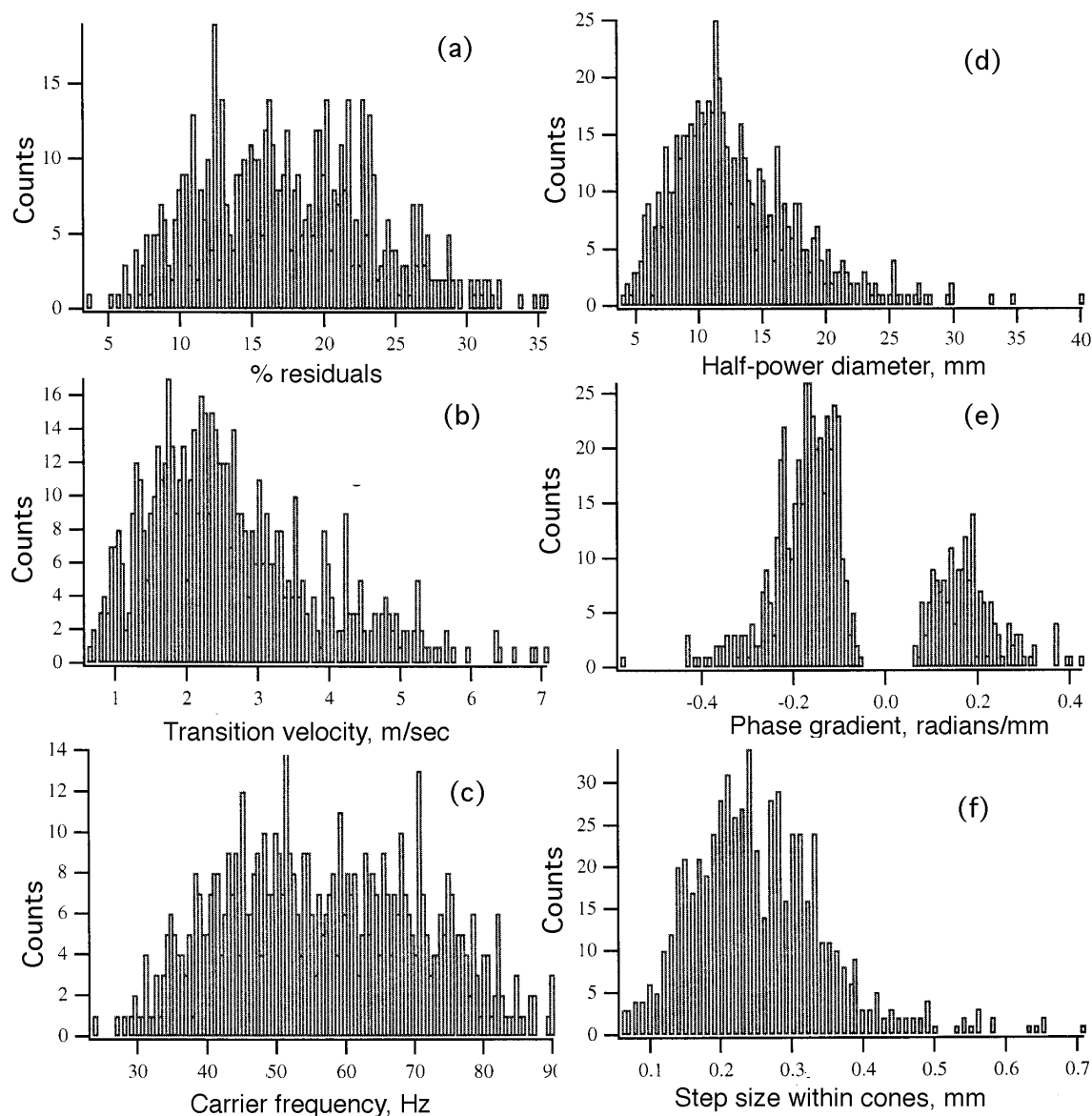


Figure 8. The histograms show selected properties of phase cones from a typical subject and site (here visual cortex). A summary over subjects is given in Table 2. The values were compiled from stable phase cones after screening for minimal EEG % residual, minimal duration, and maximal drift but not by thresholds for carrier frequency, cone % residual, or half-power diameter in mm. By definition all cones had diameters of $\sqrt{2}$ radians, but cones with higher carrier frequency had higher velocity, hence larger diameter.

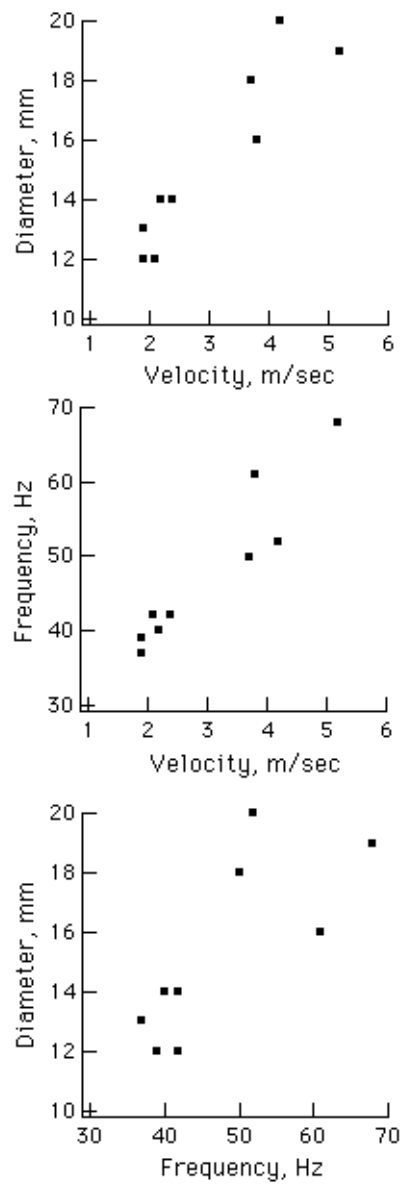


Figure 9. The relations are shown between carrier frequency (f), transition velocity (v), and half-power diameter (d). The three ordinary correlation coefficients were:

$$r_{vd} = .93; r_{vf} = .94; r_{fd} = .76.$$

The partial correlation coefficients were:

$$r_{pvd} = .93; r_{pvf} = .94; r_{pfd} = -.79.$$

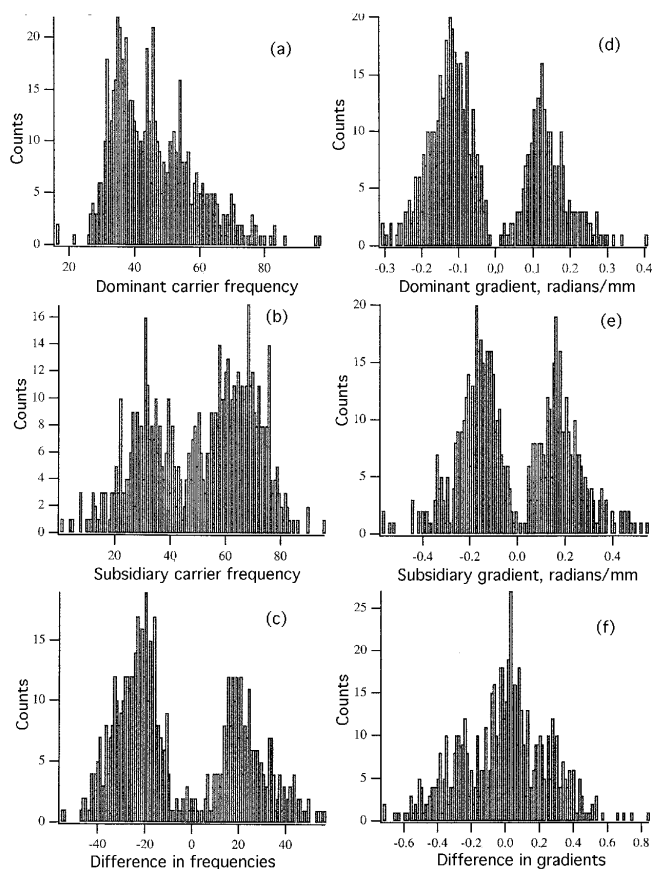


Figure 10. The properties are compared of phase cones derived from the dominant (larger) and subsidiary (smaller) wavelets successfully fitted in the same segments by nonlinear regression. Whereas the phase cones of the two components invariably had the same location and sign of the apices, the two components from neocortical EEGs differed in apical sign and location by as much as did successive phase cones of the dominant component, suggesting that the neocortices can sustain multiple wave packets simultaneously.

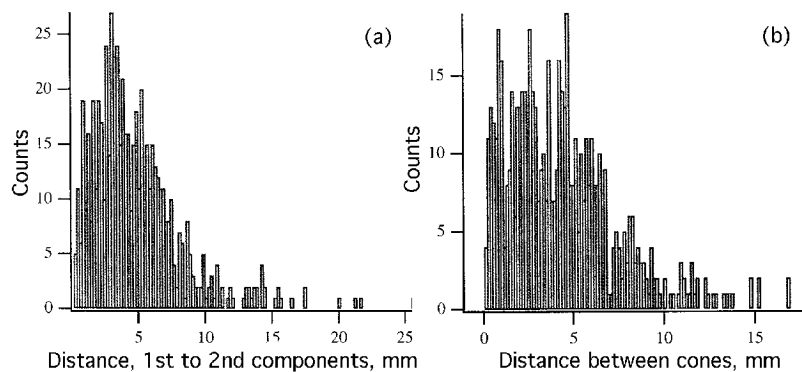


Figure 11. The distributions are compared of (a) the distances between the apices of the cones derived from the dominant versus subsidiary wavelets within segments and (b) the distances between the apices of successive pairs of dominant cones in the same subject. Similar results were found in all 9 subjects. For both data sets the distances between the apices of stable cones were substantially greater than the maximal drifts within stable cones but much less than the half-power diameters of the cones (Table 3).

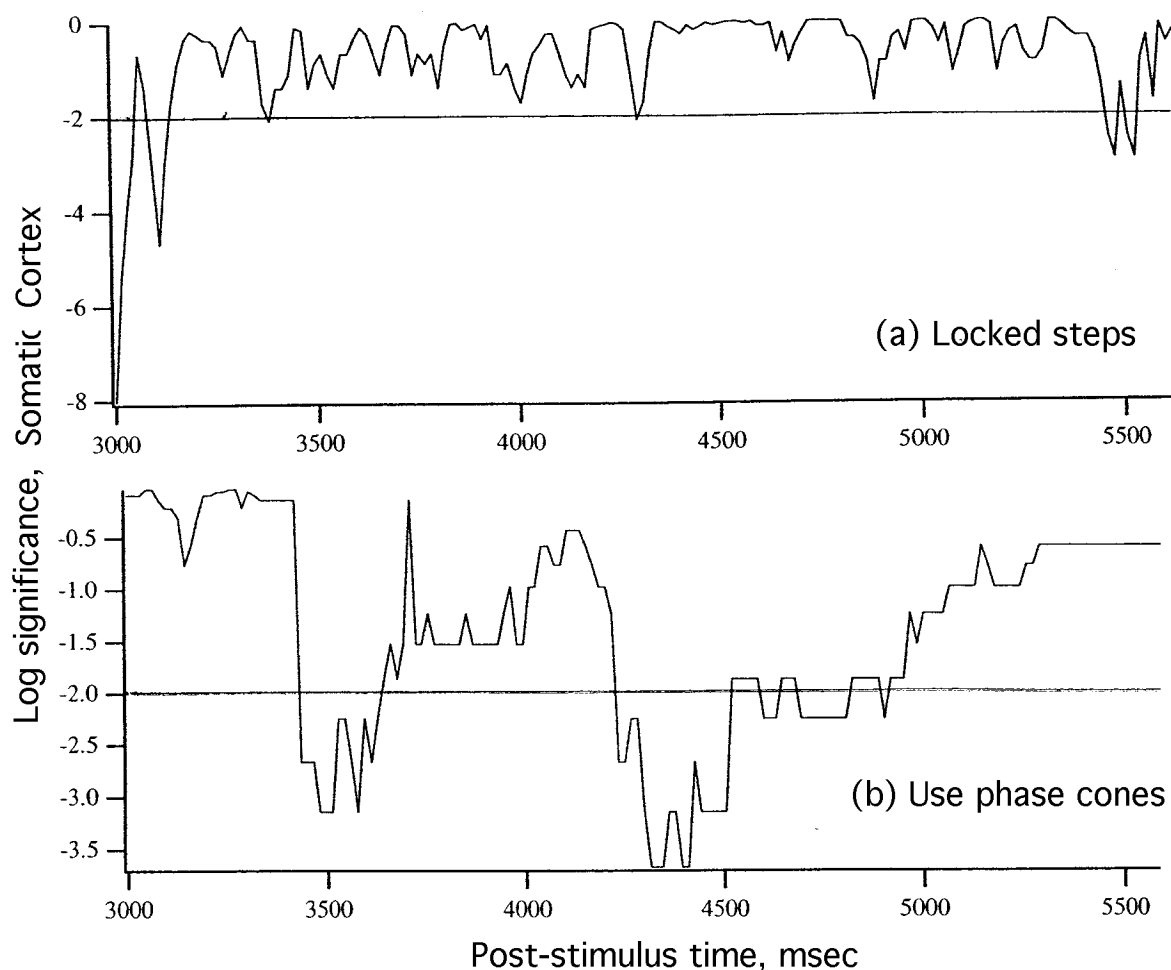


Figure 12. The probability of correct classification by chance of AM patterns from the visual cortex with respect to CS+ and CS- across 20 trials of each was calculated for 64 msec segments in windows overlapped in 16 msec steps (a) locked to the time of CS onset across all trials versus (b) taking instead RMS segments adjacent to the nearest phase cones before or after the fixed step on all trials. The results are shown for a representative trial set from one subject. The lines show the level of $p = .01$.

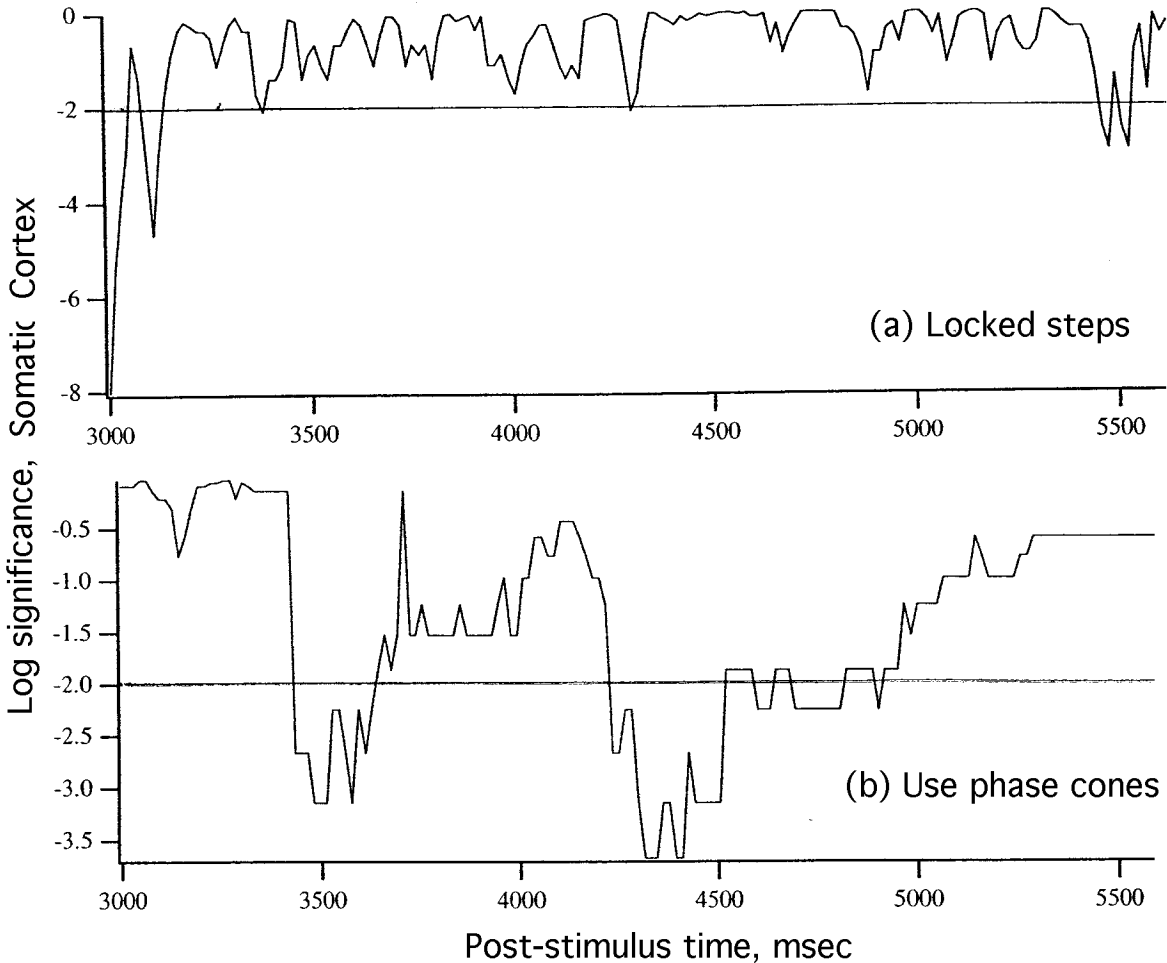


Figure 13. An example as in Figure 12 is shown from the auditory cortex of another subject.

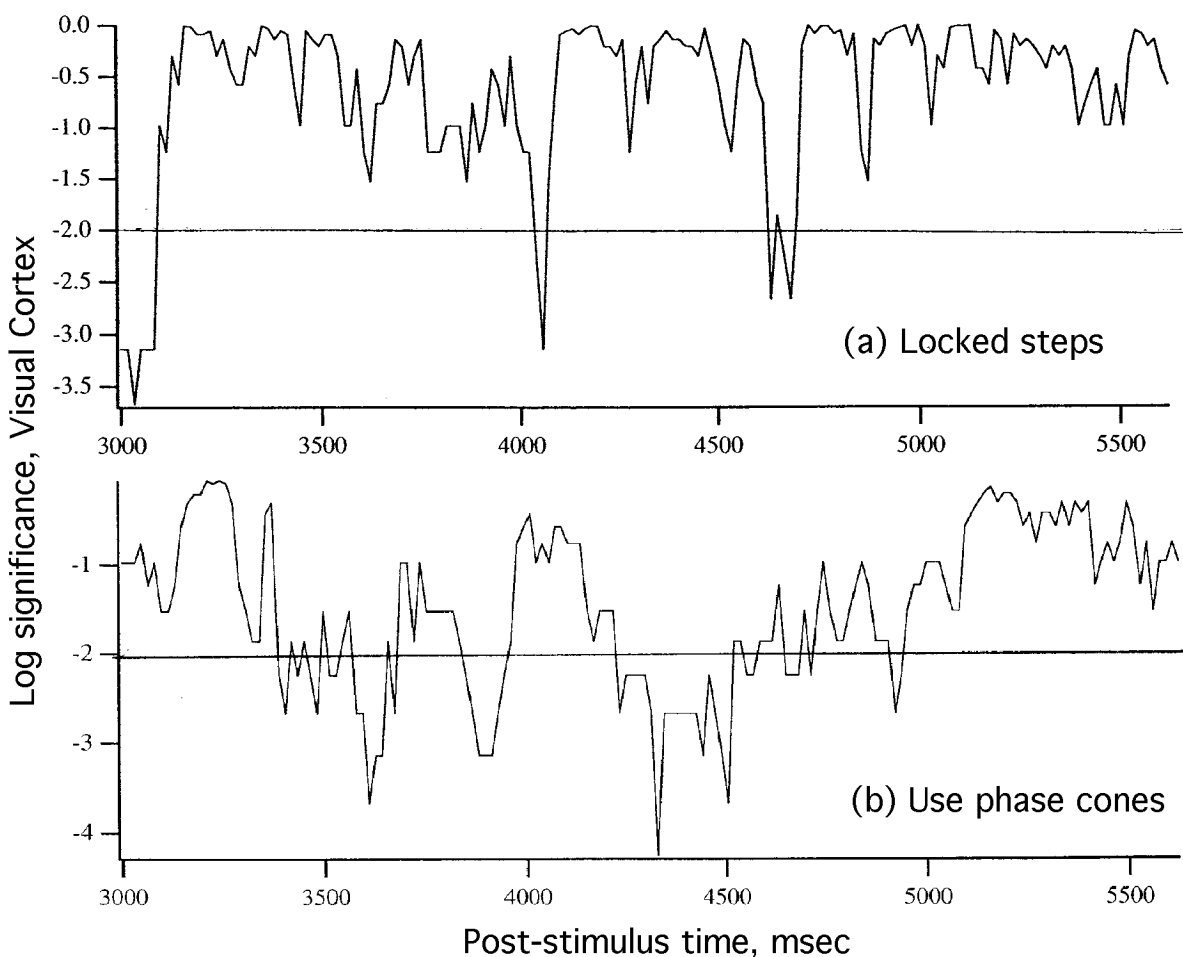


Figure 14. An example as in Figure 12 shows from the somatomotor cortex of another subject.

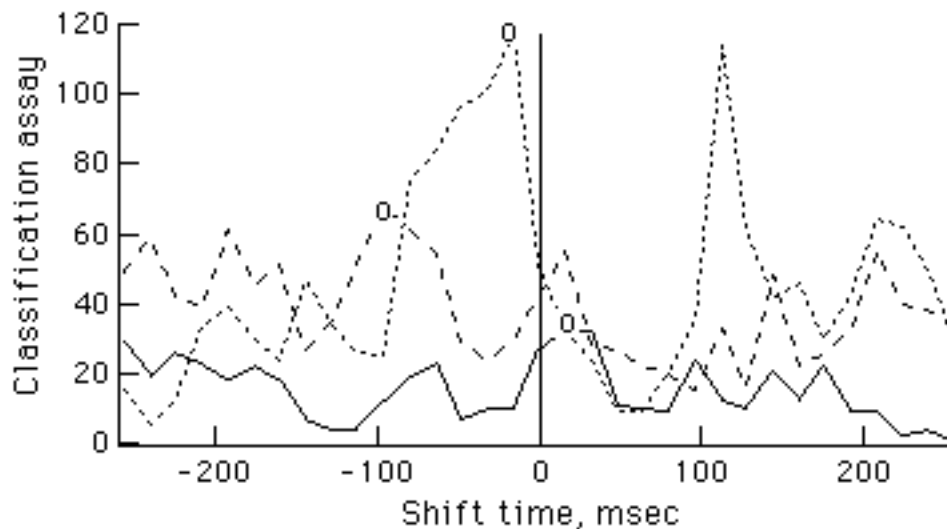


Figure 15. Three examples are shown of the effects on an over-all classification assay (number of steps at which the probability of correct classification of AM patterns by chance $p < .05$) of shifting the entire RMS data base by the designated time increments in steps of ± 16 msec. Mean values of the optimal shifts (o) in msec are listed in the right-most column in Table 2.

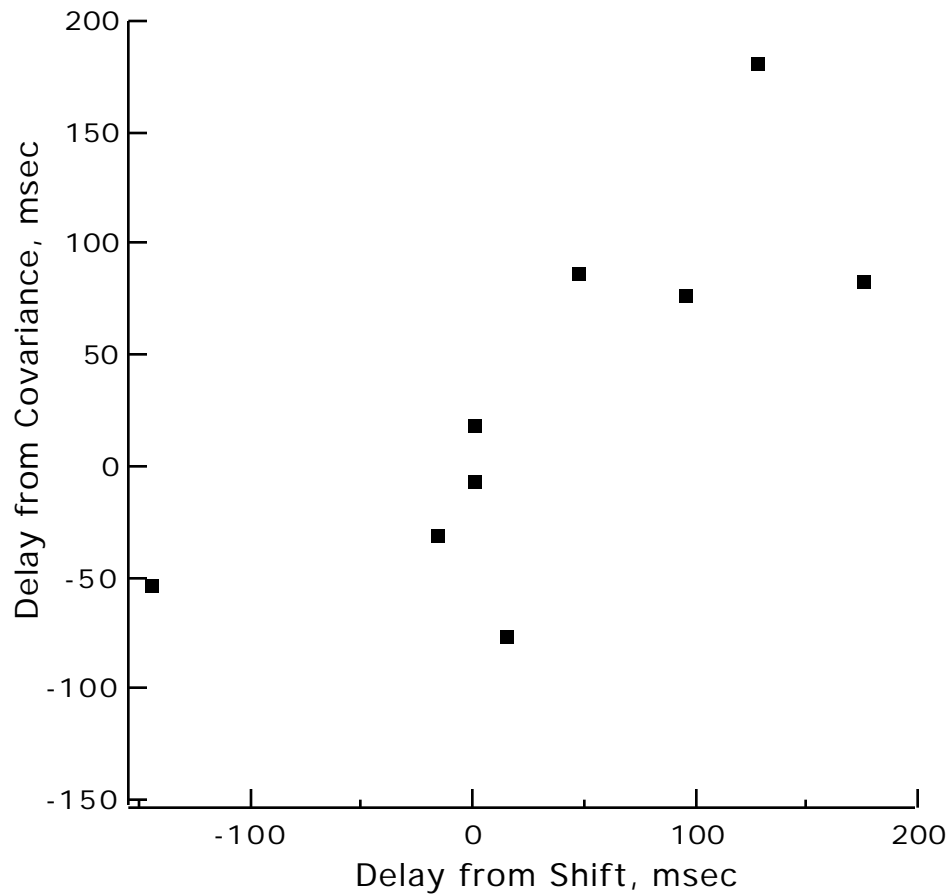


Figure 16. The estimates of the shift times of the RMS segments with respect to the times of onset of the phase cones after optimization of the classification assay with respect to behavior (abscissa) are compared with the estimates of lag times (ordinate) derived by the phase at the peak of the cross-spectrum of the covariance between the appearance of the phase cones (Figure 6) and the spatial ensemble average EEG (Table 2). The correlation coefficient between these independently derived estimates was 0.82.

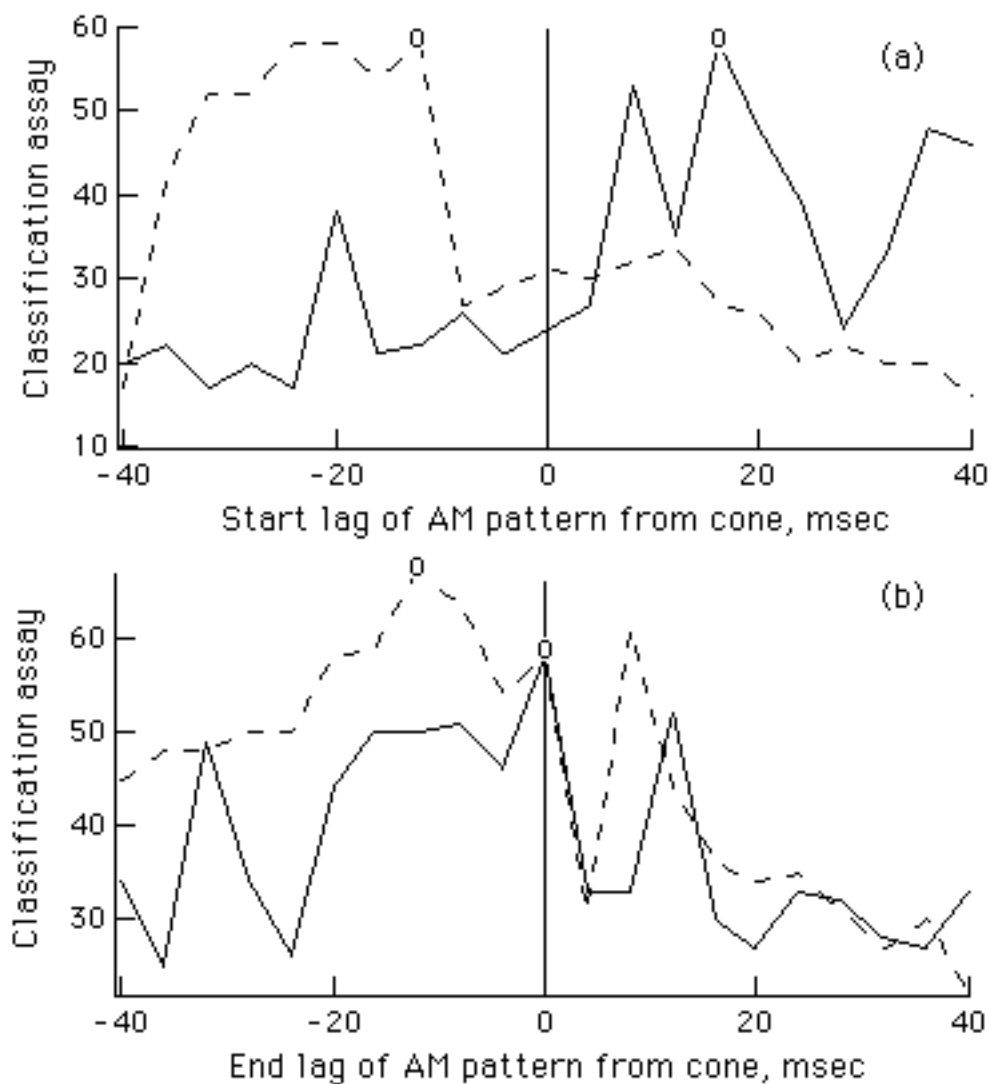


Figure 17, a. Two examples are shown of how varying the start times at which the calculation of the onset of RMS distribution with respect to the times of onset of phase cones changed the over-all classification assay.

b. The relations are shown of the times of ending of RMS segments with those of the stable cones. The results combined with those summarized in Table 2 and Figure 15 suggest that an identifiable AM pattern forms within 30 msec after a cortical state transition and persists 80 to 100 msec until both the AM and PM patterns dissolve. For modal frequencies this delay is between one and two cycles of the gamma oscillations.